THE JOURNAL OF BIOLOGICAL CHEMISTRY
Vol. 271, No. 31, Issue of August 2, pp. 18632–18637, 1996
© 1996 by The American Society for Biochemistry and Molecular Biology, Inc.
Printed in U.S.A.

Characterization of the Mononickel Metallocenter in H134A Mutant Urease*

(Received for publication, February 8, 1996, and in revised form, April 19, 1996)

Il-Seon Park‡§, Linda O. Michel‡, Matthew A. Pearson¶, Evelyn Jabri¶‖, P. Andrew Karplus¶, Shengke Wang‡‡, Jun Dong**, Robert A. Scott**, Brian P. Koehler**, Michael K. Johnson**, and Robert P. Hausinger‡§§**

*From the ‡Departments of Microbiology and Biochemistry, Michigan State University, East Lansing, Michigan 48824-1101, the ¶Section of Biochemistry, Molecular and Cell Biology, Cornell University, Ithaca, New York 14853-2703, and the **Departments of Chemistry and Biochemistry and Molecular Biology and the Center for Metalloenzyme Studies, University of Georgia, Athens, Georgia 30602-2556*

A mutant form of *Klebsiella aerogenes* urease possessing Ala instead of His at position 134 (H134A) is inactive and binds approximately half the normal complement of nickel (Park, I.-S., and Hausinger, R. P. (1993) *Protein Sci.* 2, 1034–1041). The crystal structure of the H134A protein was obtained at 2.0-Å resolution, and it confirms that only Ni-1 of the two nickel ions found in the native enzyme is present. In contrast to the pseudotetrahedral geometry observed for Ni-1 in native urease (where it is liganded by His-246, His-272, one oxygen atom of carbamylated Lys-217, and a water molecule at partial occupancy), the mononickel metallocenter in the H134A protein was found to possess octahedral geometry and was coordinated by the above protein ligands plus three water molecules. The nickel site of H134A urease was probed by UV-visible, variable temperature magnetic circular dichroism, and x-ray absorption spectroscopies. The spectroscopic data are consistent with the presence of Ni(II) in octahedral geometry coordinated by two histidylimidazoles and additional oxygen and/or nitrogen donors. These data underscore the requirement of Ni-2 for formation of active urease and demonstrate the important role of Ni-2 in establishing the proper Ni-1 coordination geometry.

Urease (EC 3.5.1.5) is a nickel-containing enzyme that catalyzes the hydrolysis of urea (1, 2). In addition to playing a key role in plant (3) and microbial (4) nitrogen metabolism, the enzyme has been implicated as a virulence factor in various human and animal pathogens (reviewed in Ref. 2). The three-dimensional structure has been resolved to 2.2 Å (5) for the best characterized urease, that from the enteric bacterium *Klebsiella aerogenes*. The protein is a trimer of trimers ($(\alpha\beta\gamma)_3$) composed of subunits with M_r = 60,304 (α), 11,695 (β), and 11,086 (γ). The enzyme active site is located in the α-subunit and contains a binickel center in which the two metal ions are separated by 3.5 Å and bridged by carbamylated Lys-217. In the crystallographic model, one nickel ion (Ni-2) exhibits distorted trigonal bipyramidal or distorted square pyramidal geometry in which two nitrogen ligands are derived from His-134 and His-136, and three oxygen atoms are contributed by carbamylated Lys-217, Asp-360, and a solvent molecule (Wat-1).[1] The second urease metal ion (Ni-1) exhibits pseudotetrahedral geometry, a coordination that is unusual for nickel. The ligands to Ni-1 include the second oxygen atom of the carbamylated Lys-217, nitrogen atoms from His-246 and His-272, and partial coordination to the solvent molecule that is strongly coordinated to Ni-2.

In an effort to better characterize the novel coordination geometry observed in the Ni-1 site of urease, we have examined a mutant with His-134 substituted by Ala (H134A) that contains only this metal ion (6). We compare the crystal structure and the UV-visible, XAS, and VTMCD spectroscopic signatures of the H134A protein to the corresponding properties of the native enzyme (5, 7–9).[2] We demonstrate that the Ni-1 metallocenter geometry is perturbed in the H134A mutant protein, which lacks Ni-2, compared with that observed crystallographically for Ni-1 in the wild-type enzyme. Spectroscopic analyses of the novel H134A nickel center have proven useful in better understanding the spectra for the native enzyme, and these studies offer insight into a new biological nickel-binding site.

EXPERIMENTAL PROCEDURES

Protein Purification—The H134A protein was purified from *Escherichia coli* DH5 cells carrying the mutated pKAU17 plasmid as previously described (6). Because the enzyme was inactive, purification was monitored by sodium dodecyl sulfate-polyacrylamide gel electrophoresis. The absence of urease activity in the H134A protein was based on a colorimetric assay in which the product ammonia was converted to indophenol under standard assay conditions (7).

Crystallographic Methods—Crystals of the H134A protein were grown as described for the wild-type enzyme (10). Data collection yielded 52,421 unique reflections between infinity and 2.0 Å (96% completeness, 3.3-fold redundancy), with symmetry-related *R*-factor for

* This work was supported by the Michigan State University Agricultural Experiment Station, United States Department of Agriculture Grants 9303870 and 9503443 (to R. P. H. and P. A. K.), National Institutes of Health Grants DK45686 (to R. P. H.) and GM42025 (to R. A. S), and National Science Foundation Grant MCB9419019 (to M. K. J.). The costs of publication of this article were defrayed in part by the payment of page charges. This article must therefore be hereby marked "*advertisement*" in accordance with 18 U.S.C. Section 1734 solely to indicate this fact.

§ Present address: Dept. of Biological Chemistry and Molecular Pharmacology, Harvard Medical School, Boston, MA 02115.

‖ Present address: Dept. of Chemistry and Biochemistry, University of Colorado, Boulder, CO 80309.

‡‡ Present address: Center for Synchrotron Radiation Research and Instrumentation, Dept. of Physics, Illinois Inst. of Technology, Chicago IL 60616.

§§ To whom correspondence should be addressed: Dept. of Microbiology, 160 Giltner Hall, Michigan State University, East Lansing, Michigan 48824-1101. Tel.: 517-353-9675; Fax: 517-353-8957; E-mail: RHausing@MSU.EDU.

This is an open access article under the CC BY license.

[1] The abbreviations used are: Wat, water; XAS, x-ray absorption spectroscopy; VTMCD, variable temperature magnetic circular dichroism; α_c, calculated phase for structure factor; EXAFS, extended x-ray absorption fine structure; MCD, magnetic circular dichroism; ρ_{rms}, root mean square value for the electron density; SSRL, Stanford Synchrotron Radiation Laboratory.

[2] B. P. Koehler, K. L. Kiick, M. G. Finnegan, I.-S. Park, R. P. Hausinger, and M. K. Johnson, manuscript in preparation.

TABLE I
X-ray absorption spectroscopic data collection and reduction for H134A urease

SR facility	SSRL
Beam line	7–3
Monochromator crystal	Si[220]
Detection method	Fluorescence
Detector type	13-Element solid-state array[a]
Scan length (min)	22
Scans in average	16
Metal concentration (mM)	≈1
Temperature (K)	10
Energy standard	Ni foil (1st inflection)
Energy calibration (eV)	8333
E_0 (eV)	8342
Pre-edge background	
Energy range (eV)	8005–8297[b]
Function (width; eV)	Gaussian (1000)
Spline background	
Energy range (eV; polynomial order)	8347–8577 (3) 8577–8807 (3) 8807–9037 (3)

[a] The 13-element germanium solid-state x-ray fluorescence detector at SSRL was provided by the National Institutes of Health Biotechnology Research Resource.

[b] Background was fitted in this region and then extrapolated to the whole data region. This background was then subtracted from raw XAS data.

all data of 6.6%. The initial model was constructed starting with the refined coordinates of *K. aerogenes* urease at 2.2-Å resolution (Ref. 5; protein data bank entry 1KAU). Difference electron density maps ($(F_{H134A} - F_{c(holourease)}, \alpha_c)$ and $(2F_{cH134A} - F_{c(holourease)}, \alpha_c)$) were used to determine the extent and position of structural changes. Guided by these electron density maps, His-134 was replaced by Ala; Ni-2, Wat-1, and Wat-170 were removed; and Wat-176, Wat-177, Wat-178, and Wat-179 were added to the model with the program CHAIN (11). This adjusted model was refined against all data between 10.0 and 2.0 Å by using the conventional positional and restrained individual *B*-factor refinement protocols in XPLOR (12), followed by manual fitting to $2F_o - F_c$ maps. In the final stages of refinement, residues 317–331 were removed from the model as they had electron density less than 0.5 times the root mean square level. The final model, with an *R*-factor of 17% for all data ($\sigma > 0$) between 10.0 and 2.0, included 752 amino acid residues, one nickel atom, and 308 water molecules. The root mean square deviations from ideality were 0.009 Å for bond lengths and 1.63° for bond angles.

UV-visible Spectroscopic Methods—UV-visible spectra of H134A mutant and wild-type ureases were obtained, and difference spectra were calculated on a Beckman DU-7500 spectrophotometer equipped with a 1.0-cm microcuvette at 25 °C. For ease in spectral comparison, data for the wild-type protein were adjusted to equal the absorbance at 280 nm of the mutant protein. Based on the known composition of the protein (13), the molar absorption coefficient at 280 nm was calculated to be 57,870 M^{-1} cm^{-1} (14), and the concentration of the mutant protein used for spectroscopy was estimated to be 14.9 mg ml^{-1}.

VTMCD Spectroscopy—VTMCD measurements over the temperature range 1.5–300 K in the UV-visible/near-IR region were carried out at a magnetic field of 4.5 teslas using an Oxford Instruments SM3 superconducting magnet mated to either a Jasco J500C (200–1000 nm) or J720 (700–2000 nm) spectropolarimeter. The experimental protocols used in the VTMCD measurements have been described in detail elsewhere (15). Samples for VTMCD studies contained 60% (v/v) glycerol to ensure formation of a glass on freezing.

XAS Methods—Ni K-edge x-ray absorption spectra of the H134A urease variant were measured on beam line 7-3 at SSRL with the SPEAR ring running at 3.0 GeV and 40–100-mA current. Details of XAS data collection and reduction are summarized in Table I. Standard EXAFS data analysis was performed (16) using EXAFSPAK software (courtesy of G. N. George). Curve-fitting was carried out on the raw EXAFS data in which single and multiple scattering paths within ~4.5 Å of the nickel atom were included to identify and quantify His-imidazole coordination. FEFF Version 5.05 (17–19) was used to calculate scattering amplitudes and phase shifts for each scattering path containing four or fewer legs. Coordination numbers were constrained to be integer, and the effective distances and Debye-Waller factors for outer-shell atoms of imidazole rings were constrained to a given ratio with the first-shell (nickel–nitrogen/oxygen) distance and Debye-Waller factor, respectively. This type of analysis typically yields first-shell distances with an accuracy of ±0.02 Å.

RESULTS AND DISCUSSION

H134A mutant urease was purified as described previously (6). This protein was devoid of urease activity (<0.001 unit mg^{-1}) (6), even when chemical rescue was attempted by incubation with imidazole and nickel ions. The protein was structurally characterized by x-ray diffraction methods and spectroscopically examined as described below.

Crystal Structure of H134A Urease—The final electron density map of H134A urease (Fig. 1*A*) clearly defines the structure of the novel metallocenter in this protein. Compared with the binickel center of the native enzyme, Ni-2 is missing in the mutant protein due to the loss of the His-134 ligand. Ni-1 remains bound and well ordered (B = 24 Å^2 in the H134A protein *versus* B = 18 Å^2 in the wild-type enzyme), but is shifted by 0.5 Å. Notably, Lys-217 is carbamylated in the mutant protein. The coordination sphere around Ni-1 has changed from the tricoordinate, approximately tetrahedral geometry found in the native enzyme (5) to hexacoordinate, approximately octahedral geometry in the H134A protein. The six ligands coordinating Ni-1 in the mutant protein include the three ligands found in the wild-type protein structure (His-246, His-272, and carbamylated Lys-217) and three new water molecules (Wat-176, Wat-177, and Wat-179). Two of the solvent ligands (Wat-176 and Wat-177) are well ordered (B = 15 Å^2) and have strong density, while the third (Wat-179) is less ordered (B = 37 Å^2) and consequently has weaker density. Another water molecule, Wat-178 (B = 26 Å^2), is not a Ni-1 ligand, but is present near the metal site and acts as a hydrogen-bonding partner to Wat-176. It is interesting to note that a 2.5-Å resolution data set collected from a smaller crystal did not show evidence of the new water molecules. We suspect that this is due to Fourier transform series termination errors around the electron-dense nickel site. Selected distances and ligand-metal-ligand angles (all within 13° of being orthogonal) are shown in Table II. Consistent with the idea that individual metal-ligand interactions grow weaker as more ligands surround the metal ion (20), the distances between Ni-1 and the protein ligand atoms are increased compared with the native enzyme. The Ni-1–O–C angle associated with the carbamylated lysine ligand is 123° in the mutant protein structure *versus* 132° in the wild-type protein. This shift in orientation may allow for improved interactions between the single metal and the lone-pair electrons on the carbamylated Lys carbonyl oxygen in the H134A protein compared with the native enzyme, where coordination of the second carbamate oxygen to Ni-2 causes additional constraints. As shown by a comparison of the H134A model with that of wild-type urease (Fig. 1*B*), no residue near the metallocenter shifts by more than 0.5 Å. This result is consistent with the near absence of changes in the apoprotein structure[3] and indicates that the protein ligands are preorganized, perhaps related to the tight binding of nickel to urease. As expected, the ordered water structure changes at the metallocenter. Several new stabilizing hydrogen bonds are illustrated in Fig. 1*B* (distances are provided in Table II). One interesting interaction is a new hydrogen bond between Asp-360 and His-136, which appears to stabilize their close approach in the absence of Ni-2.

The protein structures for the H134A and native enzymes are nearly identical, except for residues 314–331, a flap that covers the metallocenter. For example, the root mean square deviation is 0.14 Å when comparing the 749 C-α positions not

[3] E. Jabri and P. A. Karplus, manuscript in preparation.

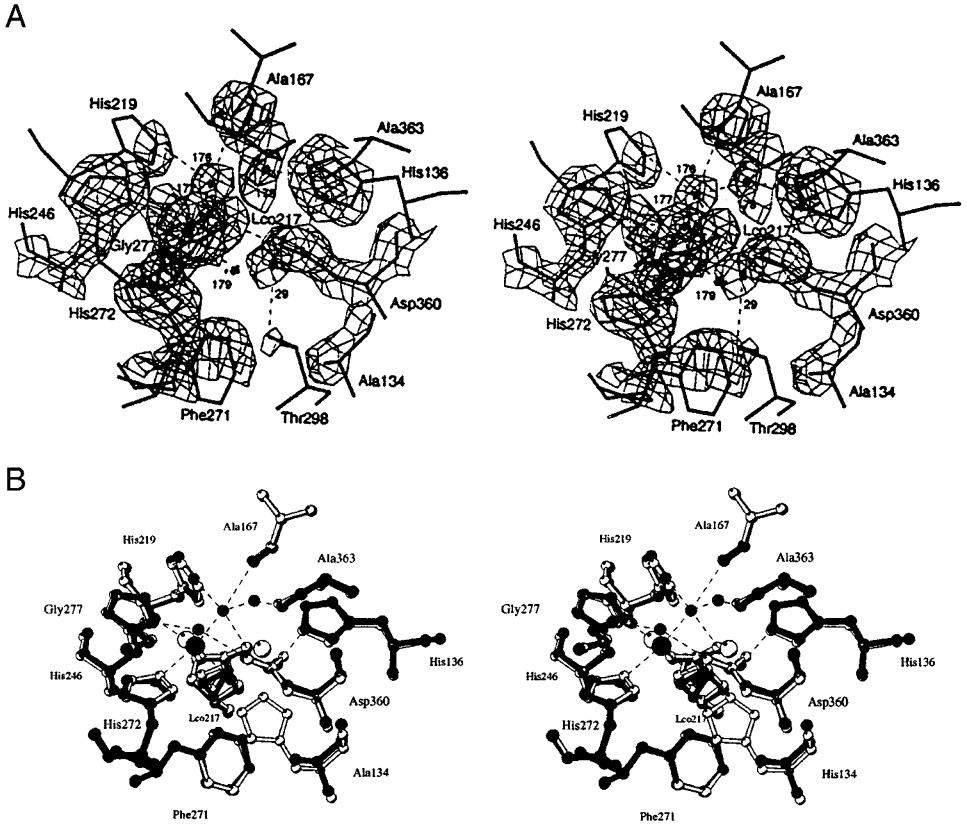

FIG. 1. **Structure of the *K. aerogenes* H134A metallocenter.** *A*, stereodiagram of the mononickel center showing the octahedral geometry around Ni-1. The view is looking down on the metal center with carbamylated Lys-217 (*Lco217*) behind the metal center. Wat-176, Wat-177, Wat-178, and Wat-179 are solvent molecules. The electron density (calculated using coefficients $2F_o - F_c$, α_c) is contoured at 1.2 ρ_{rms}. *B*, overlay stereodiagram of the active-site residues of H134A urease (*black*) and wild-type urease (*white*). The view is slightly rotated relative to *A*, but the orientations of Ni-1 and the solvent molecules are the same. The nickel atoms (*larger spheres*) are included for both models, whereas the active-site water molecules are included only for the H134A protein. Metal coordination bonds and hydrogen bonds are shown as *dashed lines*.

TABLE II
Geometry of the mononickel center of H134A urease

Distances between selected atoms are presented for H134A urease and the Ni-1 site of the wild-type enzyme. Angles are presented only for the H134A protein. His-246, His-272, and carbamylated Lys-217 (Lys*217) are ligands of Ni-1 in native urease, while Wat-176, Wat-177, and Wat-179 are additional ligands in the H134A structure.

–	Interatomic distance		H134A ligand-metal-ligand angles	Angles
	H134A	Native		
	(Å)	*(Å)*		*(Å)*
Ni-1–Lys*217 $O^{\theta 1}$	2.3	2.1	Lys*217 O^{θ}–Ni-1–His-272 N^{ϵ}	103
Ni-1–His-272 N^{ϵ}	2.6	2.3	Lys*217 O^{θ}–Ni-1–His-246 N^{δ}	84
Ni-1–His-246 N^{δ}	2.4	2.0	Lys*217 O^{θ}–Ni-1–Wat-176	82
Ni-1–Wat-176	2.2		Lys*217 O^{θ}–Ni-1–Wat-179	79
Ni-1–Wat-177	2.0		Wat-177–Ni-1–His-272 N^{ϵ}	90
Ni-1–Wat-179	2.3		Wat-177–Ni-1–His-246 N^{δ}	100
Wat-176–Lys*217 $O^{\theta 2}$	2.6		Wat-177–Ni-1–Wat-176	86
Wat-176–Wat-178	2.4		Wat-177–Ni-1–Wat-179	98
Wat-176–Ala-167 O	2.9		Wat-176–Ni-1–Wat-179	96
Wat-176–His-219 N^{ϵ}	2.8		Wat-179–Ni-1–His-272 N^{ϵ}	94
Wat-177–Gly-277 O	2.4		His-272 N^{ϵ}–Ni-1–His-246 N^{δ}	84
Wat-177–Asp-360 $O^{\delta 2}$	2.9		His-246 N^{δ}–Ni-1–Wat-176	88
Wat-178–Ala-363 O	3.0			
Wat-179–Asp-360 $O^{\delta 1}$	2.7			
His-136 N^{ϵ}–Asp-360 $O^{\delta 1}$	2.7	3.0		

associated with this flap. The structure of this flap region in the mutant protein, however, is highly disordered. Residues 314–316 shift by ~1 Å, and the rest of this flap, residues 317–331, become sufficiently disordered that we have removed them from the model. Part of the disorder in this region may arise from the absence of Wat-170 in the H134A structure. In the native enzyme, Wat-170 hydrogen bonds to His-320 and may help to anchor the flap. Thus, changes in the water structure resulting from loss of Ni-2 may be reflected in increased disorder in the flap region, but otherwise do not perturb the backbone structure.

Spectroscopic Analysis of H134A Urease—The UV-visible spectrum of the H134A mutant protein is featureless beyond the absorption bands arising from the aromatic residues, whereas that of wild-type urease possesses shoulders at ~325 and ~400 nm (Fig. 2*A*). A distinct, albeit weak, absorption band at 406 nm was previously reported for the wild-type enzyme (7), but was not observed here. This absorbance feature

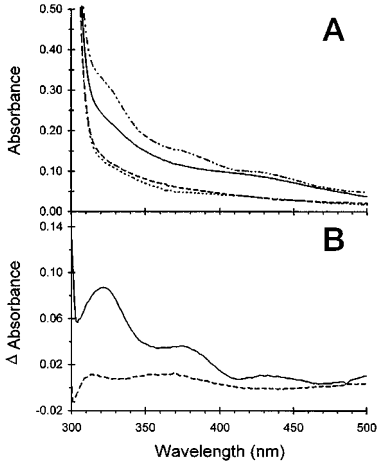

FIG. 2. **Comparison of wild-type and H134A mutant urease UV-visible spectra.** *A*, spectra of wild-type (——) and H134A (· · · ·) ureases (14.9 mg ml^{-1}) in 100 mM HEPES buffer, pH 7.75, containing 10 mM EDTA and in buffer containing 5.0 mM β-mercaptoethanol (– · · – and – – –, respectively). *B*, protein-thiol complex minus protein difference spectra for the wild-type (——) and H134A (– – –) proteins.

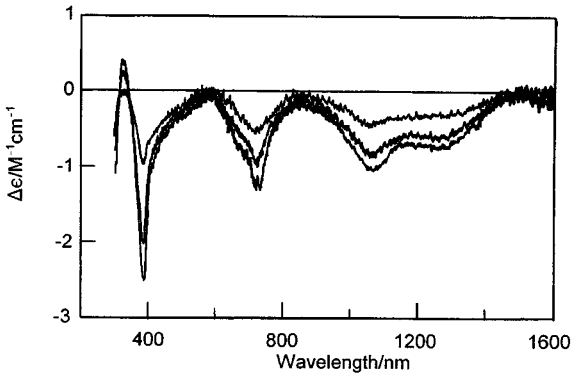

FIG. 3. **Variable temperature MCD spectra of the H134A mutant urease protein.** The sample was as used for x-ray absorption studies except for the adjustment by an additional 30% (v/v) glycerol. The spectra were recorded with a magnetic field of 4.5 teslas at 1.8, 4.2, and 9.8 K. All MCD bands increase in intensity with decreasing temperature. Δε values are based on the Ni(II) concentration assuming one Ni(II)/αβγ-unit.

is likely due to contamination by a non-urease chromophore since we noted a similar 406 nm peak in incompletely purified H134A urease samples (data not shown). As illustrated by the difference spectrum shown in Fig. 2*B* and consistent with earlier results (7), β-mercaptoethanol forms a thiolate → Ni(II) charge transfer complex with the urease metallocenter. This complex exhibits transitions at 322, 374, and ~430 nm as well as at ~750 nm (data not shown). In contrast, the addition of β-mercaptoethanol had little effect on the spectrum of the H134A protein. This result may indicate that the spectrum observed for the β-mercaptoethanol-bound enzyme arises only from a thiolate bridging the two nickel ions at the active site, as previously proposed on the basis of XAS studies (8). Because the flap covering the metallocenter is highly disordered, we discount the alternative possibility that the thiol cannot gain access to the mononickel center.

While Ni(II) ligand field bands are too weak to be seen in the absorption spectrum, they can be located in the VTMCD spectrum. VTMCD measurements down to liquid helium temperatures provide an optical probe for paramagnetic metal centers and have been used effectively to probe the electronic properties of paramagnetic Ni(II) centers in native urease (9),[2] the UreE protein (21), nickel-substituted rubredoxin (22), and a

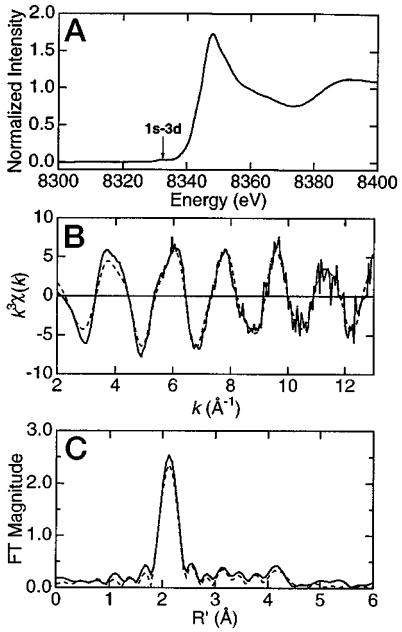

FIG. 4. **Ni K-edge XAS data for H134A urease.** *A*, Ni K-edge region showing the 8332-eV 1s → 3d transition; *B*, nickel EXAFS spectrum (——) and best-fit simulation (– – –) (Fit 6 in Table III); *C*, Fourier transforms (*FT*) of the nickel EXAFS spectrum (——) and simulation (– – –) shown in *B* (fast Fourier transforms were performed over the k = 2–13 $Å^{-1}$ range with a rectangular window and k^3 weighting).

range of nickel-substituted zinc enzymes and octahedral coordination complexes (23). Fig. 3 shows VTMCD spectra in the UV-visible/near-IR region for the H134A mutant protein at temperatures between 1.8 and 10 K with a magnetic field of 4.5 teslas. At low temperatures, octahedral Ni(II) complexes are dominated by negative temperature-dependent MCD bands with maxima close to the absorption maxima of the spin-allowed *d-d* transitions (23), and the pattern of bands for the H134A mutant protein is indicative of a distorted octahedral coordination environment. The negative bands centered at 1260 and 1070 nm are assigned to a low symmetry component of the lowest energy *d-d* band ($^3A_{2g} \rightarrow {}^3T_{1g}(P)$ under parent octahedral symmetry); the negative band centered at 700 nm and the shoulder at 650 nm are assigned to low symmetry components of the intermediate energy *d-d* band ($^3A_{2g} \rightarrow {}^3T_{1g}(F)$ under parent octahedral symmetry); and the negative band centered at 385 nm is assigned to the highest energy *d-d* band ($^3A_{2g} \rightarrow {}^3T_{2g}$ under parent octahedral symmetry). The MCD intensities under comparable conditions are very similar to those of the spin-allowed *d-d* bands of other octahedral Ni(II) complexes, *i.e.* $\Delta\epsilon < -0.5\ M^{-1}\ cm^{-1}$ and $\Delta\epsilon > -3.0\ M^{-1}\ cm^{-1}$, at ~2 K and 4.5 teslas (23). Ligand field analysis of the Ni(II) *d-d* transition leads to $Dq = 900 \pm 50\ cm^{-1}$ and $B = 900 \pm 50\ cm^{-1}$. Based on the ligand field parameters of a wide range of octahedral Ni(II) complexes with nitrogen and oxygen donor atoms (24), these values are consistent with no more than two His ligands. Hence, in accord with the x-ray crystal structure, the VTMCD data are indicative of a distorted octahedral Ni(II) center with mixed oxygen and nitrogen ligation.

It is clearly worthwhile to compare the VTMCD spectra of H134A mutant urease with that of the native enzyme. UV-visible VTMCD spectra of jack bean urease have been published (9), and very similar results have been observed for *K. aerogenes* urease.[2] The spectra comprise two dominant negative bands centered at 420 and 740 nm that were initially attributed to the two highest energy spin-allowed *d-d* bands of an octahedral Ni(II) center with predominantly oxygenic coordination (9). However, subsequent studies in the near-IR re-

TABLE III
Curve-fitting results for Ni K-edge EXAFS of H134A urease
Sample fitting range was for k = 2.0–13.0 Å^{-1}.

Fit	Group[a]	Shell	N_s[b]	R_{as}[c]	σ_{as}^2[d]	ΔE_0[e]	f'[f]
				(Å)	*(Å^2)*	*(eV)*	
1	Imid + N/O	Ni–N/O	(7)	2.09	0.0028	−0.7	0.080
	Imidazole	Ni–C_5	(2)	[3.09]	0.0023	[−0.7]	<0.050>
	Imidazole	Ni–C_2	(2)	[3.15]	[0.0024]	[−0.7]	
	Imidazole	Ni–C_4	(2)	[4.23]	[0.0032]	[−0.7]	
	Imidazole	Ni–N_3	(2)	[4.28]	[0.0032]	[−0.7]	
2	Imid + N/O	Ni–N/O	(6)	2.10	0.0020	−0.4	0.088
	Imidazole	Ni–C_5	(2)	[3.06]	0.0018	[−0.4]	<0.059>
	Imidazole	Ni–C_2	(2)	[3.15]	[0.0018]	[−0.4]	
	Imidazole	Ni–C_4	(2)	[4.23]	[0.0025]	[−0.4]	
	Imidazole	Ni–N_3	(2)	[4.29]	[0.0025]	[−0.4]	
3	Imid + N/O	Ni–N/O	(7)	2.09	0.0028	−0.9	0.082
	Imidazole	Ni–C_5	(1)	[3.06]	−0.0018	[−0.9]	<0.051>
	Imidazole	Ni–C_2	(1)	[3.15]	[−0.0019]	[−0.9]	
	Imidazole	Ni–C_4	(1)	[4.23]	[−0.0025]	[−0.9]	
	Imidazole	Ni–N_3	(1)	[4.28]	[−0.0026]	[−0.9]	
4	Imid + N/O	Ni–N/O	(6)	2.09	0.0020	−0.7	0.090
	Imidazole	Ni–C_5	(1)	[3.06]	−0.0019	[−0.7]	<0.060>
	Imidazole	Ni–C_2	(1)	[3.15]	[−0.0019]	[−0.7]	
	Imidazole	Ni–C_4	(1)	[4.23]	[−0.0027]	[−0.7]	
	Imidazole	Ni–N_3	(1)	[4.28]	[−0.0027]	[−0.7]	
5	N/O	Ni–N/O	(5)	2.09	0.0041	3.6	0.072
	Imidazole	Ni–N_1	(2)	2.08	0.0018	2.0	<0.042>
	Imidazole	Ni–C_5	(2)	[3.04]	[0.0026]	[2.0]	
	Imidazole	Ni–C_2	(2)	[3.14]	[0.0027]	[2.0]	
	Imidazole	Ni–C_4	(2)	[4.21]	[0.0036]	[2.0]	
	Imidazole	Ni–N_3	(2)	[4.26]	[0.0037]	[2.0]	
6	N/O	Ni–N/O	(4)	2.09	0.0031	3.8	0.078
	Imidazole	Ni–N_1	(2)	2.09	0.0015	2.2	<0.046>
	Imidazole	Ni–C_5	(2)	[3.05]	[0.0022]	[2.2]	
	Imidazole	Ni–C_2	(2)	[3.14]	[0.0022]	[2.2]	
	Imidazole	Ni–C_4	(2)	[4.22]	[0.0030]	[2.2]	
	Imidazole	Ni–N_3	(2)	[4.28]	[0.0030]	[2.2]	

[a] Group is the chemical unit defined for the multiple scattering calculation.
[b] N_s is the number of scatterers (or groups) per metal. Numbers in parentheses were not varied during optimization.
[c] R_{as} is the metal–scatterer distance. Numbers in square brackets in this and other columns are constrained to be multiple of the above values.
[d] σ_{as}^2 is a mean square deviation in R_{as}. Underlined values are physically unreasonable.
[e] ΔE_0 is the shift in E_0 for the theoretical scattering functions.
[f] f' is the normalized error (χ^2): $f' = ((\Sigma_i(k^3(\chi_{obs}(i) - \chi_{calc}(i)))^2 N)^{1/2})/((k^3\chi_{obs})_{max} - (k^3\chi_{obs})_{min})$. Numbers in angle brackets are f' for smoothed data.

gion failed to find an intense negative MCD band(s) corresponding to the lowest energy *d-d* band (predicted at ~1300 nm). Such bands are invariably present in the VTMCD spectra of octahedral Ni(II) complexes with an intensity comparable to that of the other two *d-d* bands (21, 23). Moreover, the intensity of the visible VTMCD bands was at least 3-fold that observed for octahedral Ni(II) complexes under comparable conditions. This has led to a reassignment of the VTMCD spectra of native urease and interpretation in terms of a five-coordinate Ni(II) center[2] corresponding to the crystallographically defined Ni-2 center (5). The VTMCD data for H134A mutant urease support this reassignment and provide a direct example of the VTMCD spectra to be expected for a Ni(II) center in urease with a distorted octahedral coordination environment.

XAS provides additional information regarding the electronic and molecular structure of the nickel center in the H134A protein. The integrated intensity of the 8332-eV 1s → 3d transition in the Ni K-edge x-ray absorption spectrum of H134A urease (Fig. 4*A*) is ~0.03 eV, consistent with a six-coordinate environment around the nickel atom (six-coordinate Ni(II) models exhibit integrated intensities for this peak of 0.006–0.040 eV) (25). Native urease (with a dinuclear active site) displays a 1s → 3d peak intensity of 0.058 eV (8), consistent with a lower average coordination geometry.

Curve-fitting results based on single-shell fits of Fourier-filtered first-shell EXAFS data suggest a total nickel coordination number of six or seven nitrogen/oxygen-containing ligands with an average distance of 2.09 (2) Å (data not shown). FEFF multiple scattering fits confirm this and also give best fits with two imidazole rings directly bonded to nickel, revealing a Ni(imidazole)$_2$(N/O)$_x$ coordination (x = 4 or 5) (Table III). The low Debye-Waller σ_{as}^2 values indicate that the nickel–nitrogen/oxygen distances are well ordered. Fig. 4*B* displays the comparison between raw EXAFS data and the simulation based on two imidazoles plus four other nitrogen/oxygen-containing ligands (Fit 6 in Table III); the Fourier transforms are shown in Fig. 4*C*. The highly uniform nickel–ligand distances obtained by this technique contrast with the results from the crystal structure. These differences are likely to arise from the lower resolution of the crystal structure compared with EXAFS.

Concluding Remarks—This study highlights the requirement of Ni-2 for formation of active urease and demonstrates the ability of Ni-2 to modulate the coordination geometry of Ni-1. Despite the dramatic change occurring at the metallocenter when comparing the mutant and wild-type proteins, the structure of the protein backbone remains essentially unchanged. Furthermore, Lys-217 is carbamylated in the H134A protein, establishing that carbamylation can occur in the absence of Ni-2. VTMCD spectroscopic analysis of this protein has already proven useful in better understanding the spectrum of the native enzyme.[2] Finally, our detailed characterization of this metallocenter has established an important new benchmark against which the nickel-binding sites of other proteins can be compared.

Acknowledgment—We thank Ginger Dziura for assistance with one preparation of protein.

REFERENCES

1. Hausinger, R. P. (1993) *Biochemistry of Nickel*, pp. 23–57, Plenum Publishing Corp., New York
2. Mobley, H. L. T., Island, M. D., and Hausinger, R. P. (1995) *Microbiol. Rev.* **59,** 451–480
3. Zonia, L. E., Stebbins, N. E., and Polacco, J. C. (1995) *Plant Physiol.* (*Bethesda*) **107,** 1097–1103
4. Mobley, H. L. T., and Hausinger, R. P. (1989) *Microbiol. Rev.* **53,** 85–108
5. Jabri, E., Carr, M. B., Hausinger, R. P., and Karplus, P. A. (1995) *Science* **268,** 998–1004
6. Park, I.-S., and Hausinger, R. P. (1993) *Protein Sci.* **2,** 1034–1041
7. Todd, M. J., and Hausinger, R. P. (1989) *J. Biol. Chem.* **264,** 15835–15842
8. Wang, S., Lee, M. H., Hausinger, R. P., Clark, P. A., Wilcox, D. E., and Scott, R. A. (1994) *Inorg. Chem.* **33,** 1589–1593
9. Finnegan, M. G., Kowal, A., Werth, M. T., Clark, P. A., Wilcox, D. E., and Johnson, M. K. (1991) *J. Am. Chem. Soc.* **113,** 4030–4032
10. Jabri, E., Lee, M. H., Hausinger, R. P., and Karplus, P. A. (1992) *J. Mol. Biol.* **227,** 934–937
11. Sack, J. S. (1988) *J. Mol. Graphics* **6,** 224–225
12. Brünger, A. T. (1993) *X-PLOR*, Version 3.0, Yale University Press, New Haven, CT
13. Mulrooney, S. B., and Hausinger, R. P. (1990) *J. Bacteriol.* **172,** 5837–5843
14. Pace, C. N., Vajdos, F., Fee, L., Grimsley, G., and Gray, T. (1995) *Protein Sci.* **4,** 2411–2423
15. Johnson, M. K. (1988) *ACS Symp. Ser.* **372,** 326–342
16. Scott, R. A. (1985) *Methods Enzymol.* **117,** 414–458
17. Rehr, J. J., and Albers, R. C. (1990) *Physical Rev. B* **41,** 8139–8149
18. Mustre de Leon, J., Rehr, J. J., Zabinsky, S. I., and Albers, R. C. (1991) *Physical Rev. B* **44,** 4146–4156
19. Rehr, J. J., Mustre de Leon, J., Zabinsky, S. I., and Albers, R. C. (1991) *J. Am. Chem. Soc.* **113,** 5135–5140
20. Berg, J. M., and Lippard, S. J. (1994) *Principles of Bioinorganic Chemistry*, University Science Books, Mill Valley, CA
21. Lee, M. H., Pankratz, H. S., Wang, S., Scott, R. A., Finnegan, M. G., Johnson, M. K., Ippolito, J. A., Christianson, D. W., and Hausinger, R. P. (1993) *Protein Sci.* **2,** 1042–1052
22. Kowal, A. T., Zambrano, I. C., Moura, I., Moura, J. J. G., and Johnson, M. K. (1988) *Inorg. Chem.* **27,** 1162–1166
23. Kiick, K. L. (1991) *Variable Low Temperature MCD Studies of the Nickel (II) Centers in Plant and Microbial Ureases.* M.Sc. thesis, University of Georgia, Athens, GA
24. Rosenberg, R. C., Root, C. A., and Gray, H. B. (1975) *J. Am. Chem. Soc.* **97,** 21–26
25. Colpas, G. J., Maroney, M. J., Bagyinka, C., Kumar, M., Willis, W. S., Suib, S. L., Baidya, N., and Mascharak, P. K. (1991) *Inorg. Chem.* **30,** 920–928